Understanding and Prediction of Ultra-Wide Band Channel Impulse Response Measurements

Benjamin Matthews*, Sven Ole Schmidt† and Horst Hellbrück†
Lübeck University of Applied Sciences, Germany
Department of Electrical Engineering and Computer Science
* Email: benjamin.matthews@stud.th-luebeck.de
† Email: sven.ole.schmidt, horst.hellbrueck@th-luebeck.de

***Abstract*—Recently, ultra-wide band transceiver systems have provided data transfer, timestamps and channel impulse response measurements to the user. The interpretation of the timestamps and the channel impulse response, however, is difficult and not intuitive. In simple scenarios, line of sight and non-line of sight pulses can be distinguished easily, which simplifies the reconstruction. For more complex scenarios, the interpretation remains difficult and is still an unsolved problem. In this paper, we investigate the channel impulse response measurements of the DecaWave DW1000 ultra-wide band transceiver and model the expected results for simple scenarios based on information provided from the transceiver data sheet. We will show that we are able to predict the measurement results of the transceiver with acceptable accuracy by applying the model above in experiments.**

***Index Terms*—channel impulse response, ultra-wide band, channel estimation, internet of things**

I. Introduction and Related Work

For the Internet of Things (IoT), ultra-wide band (UWB) communication is a promising alternative compared to existing narrow-band or spread spectrum solutions. In contrast to other IEEE 802.15.x solutions, UWB is very resilient against multipath propagation [1]. The reason is that due to large bandwidth, symbols are much shorter compared to a smaller bandwidth. Consequently, individual path components due to reflections do not overlap and this reduces the effects of inter symbol interference. Combining the short pulses with high speed clocks and time measurement units, the transceiver provides precise time-of-flight measurements, which are applied in various localization systems, like [2] and [3].

For spread spectrum technologies, pilot symbols are sent to estimate the current multipath channel in an OFDM System in [4], which is also an option for UWB systems. In [5], Zhou et. al. apply a stochastic approach to predict the current channel impulse responses (CIR) in a high-speed railway. In [6] and [7], the authors show how to generate keys for security and private transmissions from CIR measurements. Additionally, the channel information is an important optimization criterion during the installation of wireless communication systems [8]. In summary, the CIR serves various purposes in different application fields.

Consequently, we investigate CIRs as a feature of an UWB transceiver which is called *CIR data*. The CIR data from the transceiver is a result of the transmitted signal, which is affected by the wireless channel and its corresponding multipath spreading, as well as some signal processing performed by the hardware.

The contributions of the paper are:

- We develop a generalized model for wireless UWB propagation.
- We propose a new estimation of the CIR data called the *forward method*.
- We evaluate the approach with measurements.

The rest of the paper is organized as follows. Section II introduces our generalized model for the wireless UWB propagation. Our main contribution, the estimation of the CIR data, called the *forward method*, is proposed in Section III. Section IV provides a comparison of the estimated received signal with measurements. Section V concludes the paper and gives an outlook on future work.

II. Model for UWB signal propagation

This section introduces the transmission characteristics of wireless UWB transceivers and shows how the received signal is affected by multipath propagation.

Assume the signal $x(t)$ is transmitted wirelessly by a tag in a given room geometry. The signal $y(t)$, which is received by the anchor, is a superposition of multiple noisy and power-distinct copies of the transmitted signal, depending on the corresponding multipath propagation of the transmission channel. If the transmission channel is linear and time-invariant (LTI) and includes noise, the received signal $y(t)$ can be described by:

$$y(t) = x(t) * h(t) + w(t), \tag{1}$$

where $w(t) \sim \mathcal{N}(0, \sigma_n^2)$ is additive white gaussian noise.

The CIR $h(t)$ is assumed to be a superposition of N time-shifted dirac-pulses δ with individual receive power values P_{Rx}. Each of the N pulses is a single path of the multipath propagation:

$$h(t) = \sum_{i=0}^{N-1} P_{Rx,i} \cdot \delta(t - \tau_i), \tag{2}$$

where τ_i is the time shift of the signal of the i-th path.

In our investigation, the transmitted signal $x(t)$ is from an IEEE 802.15.4 compliant DecaWave DW1000 coherent UWB transceiver [9]. The CIR measurements of the transceiver are

https://doi.org/10.24355/dbbs.084-201907151207-0

presented in Section IV. Figure 1 shows the amplitude spectrum $X(f)$ of the transceiver from the datasheet, as well as the reconstructed corresponding transmitted signal $x(t)$ in the time domain.

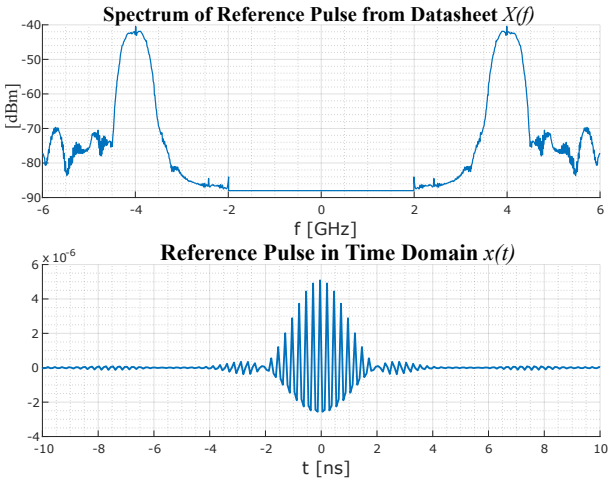

Fig. 1: Transmitted signal in frequency (top) and time domain (bottom)

The signal $x(t)$ is similar to the expected root-raised cosine reference pulse specified in the IEEE standard. Therefore, we model the transmitted signal $x(t)$ from the DecaWave transceiver as a pulse shape given in Figure 1.

The received signal $y(t)$ is processed by the hardware; mainly down-mixing and subsequently filtering. This results in a baseband signal $y_{CIR}(t)$, which is the signal provided by the transceiver hardware. Since this is the signal used to evaluate our predicted CIR, we will call it the CIR data.

III. Forward method for estimation of the CIR data

After introducing the shape of the transmitted signal $x(t)$ and the incurrence of the corresponding CIR data $y_{CIR}(t)$ in the last section, this section will show the forward method to predict this signal. Figure 2 shows a block diagram outlining the signal processing.

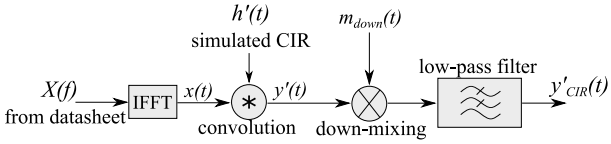

Fig. 2: Block diagram of the forward method

As shown in (2), the CIR $h(t)$ is modeled as a series of dirac pulses of varying magnitude. These pulses may be either positive or negative, depending on the individual paths of the signals. The phase of the complex transmission waves, and therefore the sign of the pulse, results from three factors: the phase offset at transmitter side, the phase based on the path length and a phase shift by π for each reflection at an obstacle.

An estimation of a CIR $h'(t)$ must be created. Ideally, this could be derived from the geometry of the room. In this case, $h'(t)$ was created with knowledge of the optimal result. The estimated received signal $y'(t)$ is calculated by convolving the reference pulse $x(t)$ with $h'(t)$. In this case, we assume a noise-free transmission with $w(t) = 0$. Figure 3 shows an exemplary CIR $h'(t)$, as well as its corresponding received signal $y'(t)$ in the time domain.

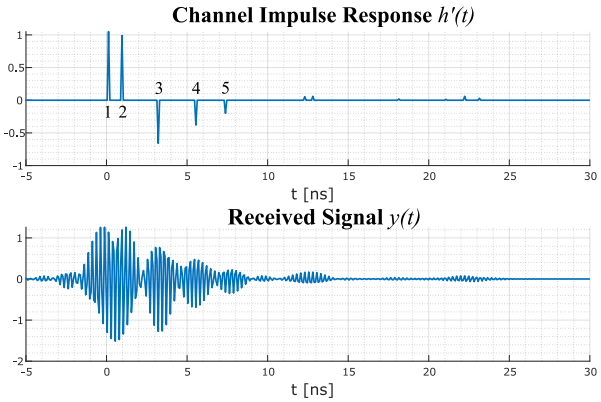

Fig. 3: Convolution of an exemplary CIR $h'(t)$ with reference pulse $x(t)$ to estimate $y'(t)$

To calculate the estimation of the CIR data, $y'(t)$ is down-converted to the baseband. In the next step, a low-pass filter eliminates irrelevant signal components from the baseband signal. This results in an estimation for the CIR data $y'_{CIR}(t)$, which is compared to $y_{CIR}(t)$ measured by the transceiver hardware in the next section.

IV. Comparison between CIR data and its prediction

The last sections described the CIR data $y_{CIR}(t)$ and its estimation $y'_{CIR}(t)$. After introducing the measurement setup in this section, we will compare these two signals.

We performed measurements in an obstacle-free space outside of a building to minimize the number of signal paths. The DecaWave transceivers were at a height of 1.35 m each and 3 m apart. When expecting a line-of sight (LOS) peak at 0 ns, the ground reflection is predicted to arrive approx. 3 ns later because the path is approx. 1 m longer. The modeled CIR is the one illustrated in Figure 3 with Peak 1 being the LOS and Peak 3 the expected ground reflection. Figure 3 shows additional peaks that we needed to add to model the measured signal correctly. Peak 2 is a path component that arrives 1 ns after the LOS which we always measure and do not have an explanation for. The path length is just 30 cm longer than the LOS path. Peaks 4 and 5 might arise from additional paths created by the measurement equipment, like the screen of the laptop, and need further investigations.

The transmission is configured to a center frequency of $f_c = 3993.6$ MHz and a corresponding bandwidth of 499.2 MHz and the measurement was captured 176 times.

https://doi.org/10.24355/dbbs.084-201907151207-0

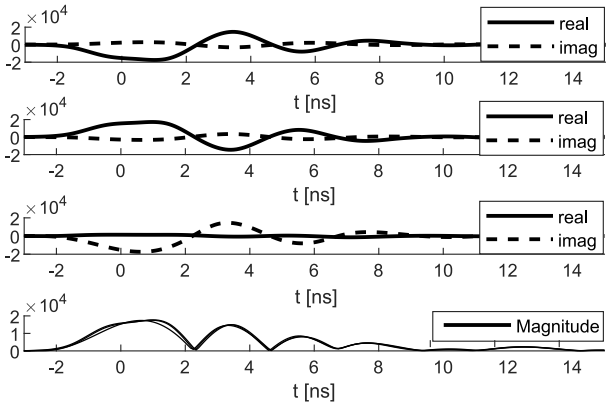

Fig. 4: Three measurements with complex components and magnitudes

Before examining the result of the convolution, we investigate the CIR data $y_{CIR}(t)$. The sampling rate of the signal is 998 MHz. Figure 4 shows a selection of three measurements of the same set up, each shifted to align at $t = 0$ ns. Since $y_{CIR}(t)$ includes phase and magnitude, each measurement provides real and imaginary components. To smooth the signal, a spline fit has been applied to each component. The plot at the bottom of the figure shows the absolute value of all three measurements.

Although the real and imaginary components of the signal change significantly from measurement to measurement, the magnitudes are nearly indistinguishable. The changes for the real and imaginary components result from varying phase offsets between the transmitter oscillator that creates $x(t)$ and the receiver oscillator. Since the offsets are unknown, the magnitude of the measurements is the simplest way to compare the measured signal to the estimated signal.

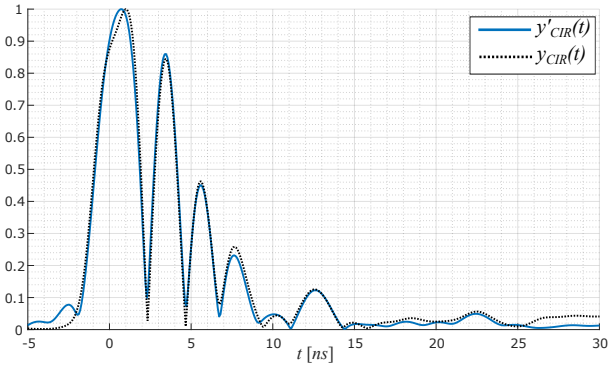

Fig. 5: Comparison of the CIR data $y_{CIR}(t)$ with its estimation $y'_{CIR}(t)$

Figure 5 shows a comparison between a single measurement of the CIR data $y_{CIR}(t)$ and the corresponding estimation $y'_{CIR}(t)$ resulting from the estimated CIR $h'(t)$.

The measurement data and the result of our estimation align very well. The shape and values of the measurements and estimation are very close as shown in Figure 5. The first peak is the line of sight peak. The second peak shows the first reflection. It supports the accuracy of this prediction.

V. Conclusion and Future Work

In this paper, we have proposed a forward method for an estimation of the CIR data $y_{CIR}(t)$. For this, we modeled the wireless UWB transmission and applied it to a baseband signal derived from the datasheet of a transceiver, based on a simulated CIR. Comparing the superimposed measurement data with our estimation depicts the accuracy of this prediction. The shape and values of the measurements and estimation are very close.

For the future, we will investigate the phase – real and imaginary part of the measurements – in more detail. We expect to retrieve additional information which means more details from the path components by these complex measurements compared to the analysis of the magnitudes in the investigation in this paper. Also, the estimation of the CIR $h'(t)$ itself is important. An improved model for the multipath propagation results in a more realistic behavior, which supports the prediction. As an implementation, we will apply the forward model and the measured CIR data in a single anchor localization system.

Acknowledgments

This publication is a result of the research of the Center of Excellence CoSA and funded by the Federal Ministry of Education & Research of the Federal Republic of Germany (Id FKZ ZF4186108BZ8, MOIN). Horst Hellbrück is adjunct professor at the Institute of Telematics of University of Lübeck.

References

[1] M. Z. Win and R. A. Scholtz, "On the robustness of ultra-wide bandwidth signals in dense multipath environments," *IEEE Communications Letters*, vol. 2, no. 2, pp. 51–53, Feb 1998.

[2] S. Krishnan, P. Sharma, Z. Guoping, and O. H. Woon, "A uwb based localization system for indoor robot navigation," in *2007 IEEE International Conference on Ultra-Wideband*, Sep. 2007, pp. 77–82.

[3] B. Grosswindhager, M. Rath, J. Kulmer, M. S. Bakr, C. A. Boano, K. Witrisal, and K. Römer, "Salma: Uwb-based single-anchor localization system using multipath assistance," in *Proceedings of the 16th ACM Conference on Embedded Networked Sensor Systems*, ser. SenSys '18, 2018, pp. 132–144. [Online]. Available: http://doi.acm.org/10.1145/3274783.3274844

[4] M. Morelli and U. Mengali, "A comparison of pilot-aided channel estimation methods for ofdm systems," *IEEE Transactions on Signal Processing*, vol. 49, no. 12, pp. 3065–3073, Dec 2001.

[5] L. Zhou, F. Luan, S. Zhou, A. F. Molisch, and F. Tufvesson, "Geometry-based stochastic channel model for high-speed railway communications," *IEEE Transactions on Vehicular Technology*, vol. 68, no. 5, pp. 4353–4366, May 2019.

[6] R. Wilson, D. Tse, and R. A. Scholtz, "Channel identification: Secret sharing using reciprocity in ultrawideband channels," *IEEE Transactions on Information Forensics and Security*, vol. 2, no. 3, pp. 364–375, Sep. 2007.

[7] P. Walther, C. Janda, E. Franz, M. Pelka, H. Hellbrück, T. Strufe, and E. Jorswieck, "Improving quantization for channel reciprocity based key generation," 10 2018, pp. 545–552.

[8] T. S. Rappaport, S. Y. Seidel, and K. Takamizawa, "Statistical channel impulse response models for factory and open plan building radio communicate system design," *IEEE Transactions on Communications*, vol. 39, no. 5, pp. 794–807, May 1991.

[9] *DW1000 IEEE 802.15.4-2011 UWB Transceiver Data Sheet*, decaWave, 2015, rev. 2.09.